

# Experimental study of geophysical and transport properties of salt rocks in the context of underground energy storage

Ismael Himar Falcon-Suarez<sup>1</sup>  | Michael Dale<sup>1,2</sup> | Hector Marin-Moreno<sup>2</sup> 

<sup>1</sup>Ocean Biogeosciences Research Group,  
National Oceanography Centre,  
Southampton, UK

<sup>2</sup>School of Ocean and Earth Science,  
University of Southampton, Southampton,  
UK

## Correspondence

Ismael Himar Falcon-Suarez, National  
Oceanography Centre, European Way,  
Southampton SO14 3ZH, UK. Email:  
isfalc@noc.ac.uk

## Funding information

European Union's Horizon 2020,  
Grant/Award Number: 765256; UK National  
Environmental Research Council,  
Grant/Award Numbers: NE/X012751/1,  
NE/X006271/1

## Abstract

Artificial caverns in salt rock formations play an important role in the net-zero energy transition challenge, both for covering short-term fluctuations in energy demand and serving as safe locations for long-term underground gas storage both for hydrogen and natural gas. Geophysical tools can serve for monitoring geomechanical changes in the salt cavern during selection and development, and during gas storage/extraction activities, but the use of common geophysical monitoring techniques has been very limited in this area. Here, we present experimental work on physical and transport properties of halite rocks within the energy storage context and assess the potential of seismic and electromagnetic data to monitor gas storage activities in salt formations. First, we analysed the stress-dependency of the elastic and transport properties of five halite rocks to improve our understanding on changes in the geological system during gas storage operations. Second, we conducted two dissolution tests, using cracked and intact halite samples, monitored with seismic (ultrasonic P- and S-waves velocities and their attenuation factors) and electromagnetic (electrical resistivity) sources to evaluate (i) the use of these common geophysical sensing methods to remotely interpret caverning development and (ii) the effect of structural discontinuities on rock salt dissolution. Elastic properties and permeability showed an increasing trend towards rock sealing and mechanical enhancement with increasing pressure for permeabilities above  $10^{-21}$  m<sup>2</sup>, with strong linear correlations up to 20 MPa. In the dissolution tests, the ultrasonic waves and electrical resistivity showed that the presence of small structural discontinuities largely impacts the dissolution patterns. Our results indicate that seismic and electromagnetic methods might help in the selection and monitoring of the caverning process and gas storage operations, contributing to the expected increase in demand of large-scale underground hydrogen storage.

## KEYWORDS

elastics, energy storage, permeability, resistivity, salt cavern

This is an open access article under the terms of the Creative Commons Attribution License, which permits use, distribution and reproduction in any medium, provided the original work is properly cited.

© 2024 The Authors. *Geophysical Prospecting* published by John Wiley & Sons Ltd on behalf of European Association of Geoscientists & Engineers.



## INTRODUCTION

Salt rock is a suitable host rock for underground gas storage (e.g. hydrogen), for disposal and storage of nuclear waste (e.g. radioactive fuel), and naturally as an effective seal for trapped oil and gas, predominantly due to excellent self-healing, low permeability, long-term creep behaviour and high entry pressures (Gloyne & Reynolds, 1961; Popp & Kern, 1998; Popp et al., 2001; Zhang et al., 2020). Salt mining for storage and extraction purposes requires a deep understanding of their in situ transport properties for the design and safety of underground cavities (i.e. to better assess the hydromechanical response of salt mine storage site during caverning development activities; Fokker, 1995; Popp & Kern, 1998). Dissolution can occur rapidly in natural (salt) karstic systems or by human activity (intentionally or inadvertently) producing impacts such as subsidence and collapse of overlying strata over a short-timescale, instability to above ground and underground construction and transport of waste out of the storage repository (Johnson, 2005; Weisbrod et al., 2012).

Halite or 'salt rock' is a highly soluble material mainly composed of sodium chloride (NaCl), but evaporite successions suitable for cavern development can also include beds of even higher solubility as carnallite and sylvite. Four requirements have been suggested for dissolution to occur (Johnson, 1989, 2005): (i) Deposits of salt through which water (brine) can flow, (ii) a source of NaCl-unsaturated brine flowing through the salt, (iii) an open outlet to allow the flow-through and (iv) enough hydraulic energy to ensure brine flow through the system. Davies (1989) described the dissolution of halite in contact with groundwater unsaturated in brine as 'essentially instantaneous', with the rate of solid salt removal controlled by diffusion and convection transport mechanisms. Transport by diffusion occurs when solutes move under the influence of their own kinetic activity in the direction of decreasing concentration. This process is slow with respect to free convection due to a contrast of pre- and post-dissolution fluid densities, which leads to more effective dissolution.

In nature, we can find natural and artificial (human-induced) salt dissolution structures. Natural dissolution is sensitive to climatic changes, as it is to groundwater. Salt karst formation in the United Kingdom was studied by Cooper (2002), who suggested that the karsting was related to changes in the groundwater regime, for example, during the last (Devensian) glaciation (Serridge & Cooper, 2022). Essentially, when the ice sheet melted, groundwater level increased and enabled the circulation of freshwater through salt units interbedded with more permeable units of siltstone, mudstone and gypsum, allowing access of fresher groundwaters to new areas of halite. Lugli et al. (1999) related the natural salt dissolution of the Messinian Realmonte salt deposit (Sicily) to basin desiccation. In this case, halite was heated upon exposure and broken and then affected by drawdown of the groundwater (~4 to 6 m below surface) with meteoric-

water dissolution cutting vertical dissolution pipes. Anderson and Kirkland (1980) found that collapse structures and breccias in the Delaware Basin of western Texas were associated with enhanced dissolution due to the free convection triggered by the density difference between the (pressurized or artesian) source of freshwater with respect to the generated brine within evaporites and collapse of overlying units. Stoeckl et al. (2020) found that the chamber collapse of abandoned salt mines in the Ukraine might increase the salinity of the Tisza river, which supplies drinking water to Ukraine, Romania, Hungary and Croatia. Moreover, salt dissolution and collapse of the Wink Sink in Texas in 1980 were found to be influenced by petroleum activities (Johnson, 1989). All these observations evidence the dynamics of unintended salt dissolution and so provide insights into the process of artificial salt dissolution and the generation of salt caverns.

Artificial salt dissolution is a common engineering approach during mining activities to enhance extraction and to generate available volumes for underground storage (i.e. generation of artificial caverns by a technique commonly referred to as 'solution-mining'; e.g. Crotogino et al., 2018; Field et al., 2019; Jiang et al., 2021; Li et al., 2020; Liu et al., 2015). The current need for an increasing use of renewable energy and developing decarbonization solutions requires specific plans for large-scale energy storage solutions (HydrogenTCP-Task42, 2023). Salt caverns are meant to play an important role in the net-zero energy transition challenge, initially covering short-term fluctuations in energy demand (e.g. Duffy et al., 2023) and serving also as safe locations for seasonal and long-term underground hydrogen storage (UHS) (Tarkowski & Czapowski, 2018). The process of solution mining and cavern formation at shallow depths (where halite is not in a plastic deformation regime) involves (i) injecting water using injection tubing to dissolve the underground salt and form brine and (ii) extracting the brine solution to surface with a production tubing set, sufficiently below the injection point to extract the higher density brine flowing downwards (Fokker, 1995). Salt cavern selection and development requires assessing potential salt damage, fracturing and containment risks from cyclic loading related to short-term seasonal fluctuations in energy demand, or land subsidence due to subsurface dissolution (Fokker, 1995; Zheng et al., 2017; Zidane et al., 2014).

Geophysical tools can be used for monitoring changes in geomechanical and fluid flow properties of the salt cavern during storage and extraction activities. Seismic properties inform about the status of the rock frame and its potential dissolution by studying changes in both P- and S-wave velocities and their respective attenuation factors. Seismic reflection data can image the internal structure of artificial caverns remotely. This possibility allows for remote monitoring and so reduces the need of intrusive approaches such as mine galleries and borehole data, which induce deformation in the salt body at different scales (Van Gent et al., 2011). Elec-

trical resistivity offers a good diagnostic of the rock changes during the caverning process due to the high conductivity contrast between the pore fluid and the rock matrix, although the poor resolution of the method in depth complicates resolving the channelling geometries accurately (e.g. Gehrman et al., 2021). The expansion of UHS activities will require the development of specific numerical predictive tools (Li et al., 2020; Yu et al., 2020), which are commonly informed by experimental observations (e.g. Jiang et al., 2021; Zheng et al., 2017). These numerical tools require constraints from laboratory tests under controlled conditions of natural salt dissolution combined with geophysical monitoring. However, due to the experimental configurations required (e.g. corrosiveness related to sample coring preparation and hypersaline fluid flow testing), these tests are complex. In addition, laboratory tests for salt rock dissolution monitoring generally use imaging techniques (e.g. Field et al., 2019) and intrusive experimental methods (e.g. Jiang et al., 2021) with no geophysical monitoring.

Experimental studies with halite rocks have historically focused on the mechanical properties and permeability characteristics of both altered (fractured) and undamaged salt rocks (e.g. Beauheim et al., 1991; Brodsky, 1994; Cosenza & Ghoreychi, 1997; Gloyna & Reynolds, 1961; Kröhn et al., 2015; Pfeifle & Hurtado, 1998; Rutqvist, 2015; Stormont, 1997; Stormont et al., 1992; Wang et al., 2018; Zhang et al., 2020). However, only few experimental works have addressed how the permeability of salt relates to P- and S-wave attributes (i.e. velocities and corresponding attenuations) under variable effective stress conditions (Ezersky & Goretsky, 2014; Popp & Kern, 1998; Popp et al., 2001). This combined analysis enables estimating remotely long-term changes in key hydromechanical properties such as pore space and connectivity with effective stress, resulting from the injection/extraction operations associated with UHS. In this regard, experimental work addressing the potential use of these tools for monitoring operational conditions post caverns development is missing, to the best of our knowledge.

Beauheim and Roberts (2002) reported salt permeabilities within the range of  $10^{-21}$ – $10^{-24}$  m<sup>2</sup> in undamaged rock formations. Popp and Kern (1998) reported a dataset combining absolute (gas) permeability with  $V_P$ ,  $V_S$  under increasing confining pressure for samples from the Gorleben salt dome (with composition ranging between 90% and 98% halite and 3% and 10% anhydrite). At low confining pressure of 5 MPa, they measured high variability in permeability ( $\sim 10^{-16}$  to  $10^{-20}$  m<sup>2</sup>), and low in P- and S-wave velocities ( $4.5 \pm 0.1$  and  $2.5 \pm 0.1$  km s<sup>-1</sup>, respectively). Within the range of 5–30 MPa, both permeability and wave velocities showed significant pressure dependency. Ezersky and Goretsky (2014) studied the relationship of porosity–permeability with the geophysical properties of shallow (within the first 50 m underground) borehole salt samples from the Dead Sea, where, since 1990, thousands of sinkholes have occurred

along coastal areas of Israel and Jordan. In this case, impurities such as carbonates filling fractures and pores (for a porosity range of 5%–21%) resulted in a higher  $V_P$  and  $V_S$  variabilities ( $4.1 \pm 0.4$  and  $2.2 \pm 0.3$  km s<sup>-1</sup>, respectively) than those reported for the Gorleben domus, and with  $V_P$ – $V_S$  decreasing approximately linearly with porosity for an equivalent permeability range of that reported by Popp and Kern (1998).

In this contribution, we analyse the hydromechanical properties of halite samples from different geological environments. The aims of this study are as follows: (i) to develop relationships between seismic-wave velocity and attenuation and transport properties of salt rocks. We also study their dependency on effective pressure to help assess suitable scenarios for UHS; (ii) to investigate salt dissolution caused by the intrusion of undersaturated brine (e.g. artificial caverning for energy storage) and the use of common geophysical sensing methods (seismic and electromagnetic tools) for monitoring the process.

## MATERIALS AND METHODS

### Rock samples

Table 1 shows the selected samples from various evaporite deposits and their main properties. From the original rock specimens, we cored  $\sim 5$  cm diameter core plugs, cut with their ends ground flat and parallel, resulting in  $\sim 2.5$  cm length samples. Rock composition was analysed by X-ray diffraction (XRD) analysis (conducted with a Philips X'Pert Pro XRD – Cu X-ray tube XRD) and connected porosity ( $\phi$ ) by He-pycnometry, whereas absolute porosity ( $\phi_T$ ) was estimated by the grain ( $\rho_s$ , from Dale, Marín-Moreno et al. (2021) and Mavko et al. (2009)) and bulk ( $\rho_b$ ) densities, according to the expression  $\phi_T = 1 - \rho_b/\rho_s$ .

### Experimental setup

The test was conducted using the high-pressure room-temperature (20°C) experimental setup for flow-through tests at the National Oceanography Centre, Southampton (Figure 1). The system allows for simultaneous measurement of the hydromechanical and geophysical properties of rock samples (e.g. Falcon-Suarez et al., 2017). Samples are radially ( $\sigma_2 = \sigma_3$ ) and axially ( $\sigma_1$ ) confined, independently controlled by a dual ISCO EX-100D system, although, for this experiment, we adopted an isotropic loading configuration (i.e.  $P_c = \sigma_1 = \sigma_3$ ). Radially, the sleeve that prevents the contact between the mineral (confining) oil and the sample is equipped with two arrays of eight electrodes each for accurate electrical resistivity (including tomography) measurements. Under our operating conditions and in homogeneous samples,

**TABLE 1** Description, physical properties and mineralogy of the rock samples, together with the stress conditions used in this study.

SampleDescription		XRD-Mineralogy (wt.%)				Bulk density	Porosity (%)		Stress path (MPa)
		Halite	Anhydrite	Polyhalite	Dolomite	(g cm <sup>-3</sup> )	Connected	Absolute	Load (unload)
S1 <sup>a</sup>	Pre-Cambrian salt from unknown well, Pakistan. Four	97.2	0	1	1.8	2.122	1.13	2.61	5
S2 <sup>a</sup>	samples collected from a commercial rock namely	97.3	0	0	2.7	2.124	1.61	2.54	10 (5)
S3	Likit salt lick bricks ( <a href="https://www.likit.co.uk/">https://www.likit.co.uk/</a> )	97.3	0	0	2.7	2.140	1.90	3.17	15 (5)
S4		97.3	0	0	2.7	2.159	1.14	2.26	5
MC	Miocene (Messinian) salt from the 3A GN3 S02 well, core 19, Sicily, Italy	95.8	0	2.2	2	2.160	0.10	1.32	10 (5)
TS	Triassic salt from Arm Hill-1 well, NW Lancashire, UK	97.6	0.2	0	2.2	2.130	0.72	1.71	15 (5)
CB	Cambrian salt from unknown well, Tunguska Basin, Russia	98.1	0	0.5	1.4	2.110	0.56	0.60	20 (5)
									30 (5)
									50 (5)

Abbreviation: XRD, X-ray diffraction.

<sup>a</sup>Samples used for the dissolution test.

the bulk electrical resistivity error is <1% for bulk resistivities <100  $\Omega$  m, increasing up to 5% with the degree of heterogeneity and above this value, at frequencies 1–500 Hz (North & Best, 2014; North et al., 2013). Axially, two platens house the ultrasonic pulse-echo sensors to measure P- and S-wave velocities ( $V_p$  and  $V_s$ ) and their respective attenuations (expressed as the inverse of their quality factor  $Q_p^{-1}$  and  $Q_s^{-1}$ ) using the pulse echo method (McCann & Sothcott, 1992). This technique provides useable frequencies between 300 and 1000 kHz, with velocity precision of  $\pm 0.1\%$  and the accuracy of  $\pm 0.3\%$  (95% confidence), and attenuation accuracy of  $\pm 0.1$  dB cm<sup>-1</sup> within this range (Best, 1992). For this test, we processed the ultrasonic data to compare the elastic properties of our samples at a single frequency of 600 kHz, obtained from Fourier analysis of broadband signals. We refer, for instance, to Falcon-Suarez et al. (2017) for further information about the instrumentation sensors specification.

For this experiment, we used two pore fluid configurations. First, we set up the rig to enable the circulation of N<sub>2</sub>-gas (directly delivered from a commercial bottle and with flow/pressure controlled by a manual regulator) through the (dry) core samples; second, during the dissolution tests, we used fluid transfer vessels (FTV1 and FTV2, Figure 1) to deliver and control (by another dual ISCO EX-100D system) the pore pressure ( $P_p$ ) using 3.5% NaCl synthetic brine solution as pore fluid.

## Halite elastic and transport properties and pressure dependency

The experiment was configured to investigate changes in the ultrasonic and transport properties of the samples under dry conditions (i.e.  $P_p \sim 0.1$  MPa). We applied a  $P_c$  loading path

of 5–10–5–15–5–20–5–30–5–50 MPa, under drained conditions, returning to the original  $P_c$  (5 MPa) to assess the increase in hysteresis (with the exception of the samples S1 and S2 used for the dissolution test; see Table 1). At every step, we applied a gentle loading/unloading stress rate of 0.05 MPa s<sup>-1</sup> up to the target  $P_c$  and then waited until the sample reached a mechanical equilibrium (i.e. when pressure controllers stabilized), before measuring the elastic and transport properties.

Elastic properties were measured using the technique and sensors described above. Permeability to N<sub>2</sub> was determined using the steady state (based on Darcy's law) and pore pressure transmission (based on transient states of the porous medium (e.g. Falcon-Suarez et al., 2017; Metwally & Sondergeld, 2011)) methods, as convenient, depending on the sample permeability; for permeabilities above 10<sup>-16</sup> m<sup>2</sup> (high-medium permeability), we used the steady state method, and for lower values the pore pressure method. To obtain the absolute permeability ( $k$ ), we applied the Klinkenberg correction (Klinkenberg, 1941) to account for the gas slippage. The uncertainty of the permeability is taken from the 95% confidence intervals of the Klinkenberg correction adjustment.

## Dissolution test procedure

Two samples were selected for the dissolution test based on their hand-scale visual features (Dale, Falcon-Suarez, et al., 2021): S1 has visible cm-scale cracks, whereas S2 is apparently coherent visually (Figure 2). To minimize potential pressure-induced changes on the original sample properties, we limited the elastic and transport characterization of these two samples to  $P_c = 15$  MPa, which was the pressure



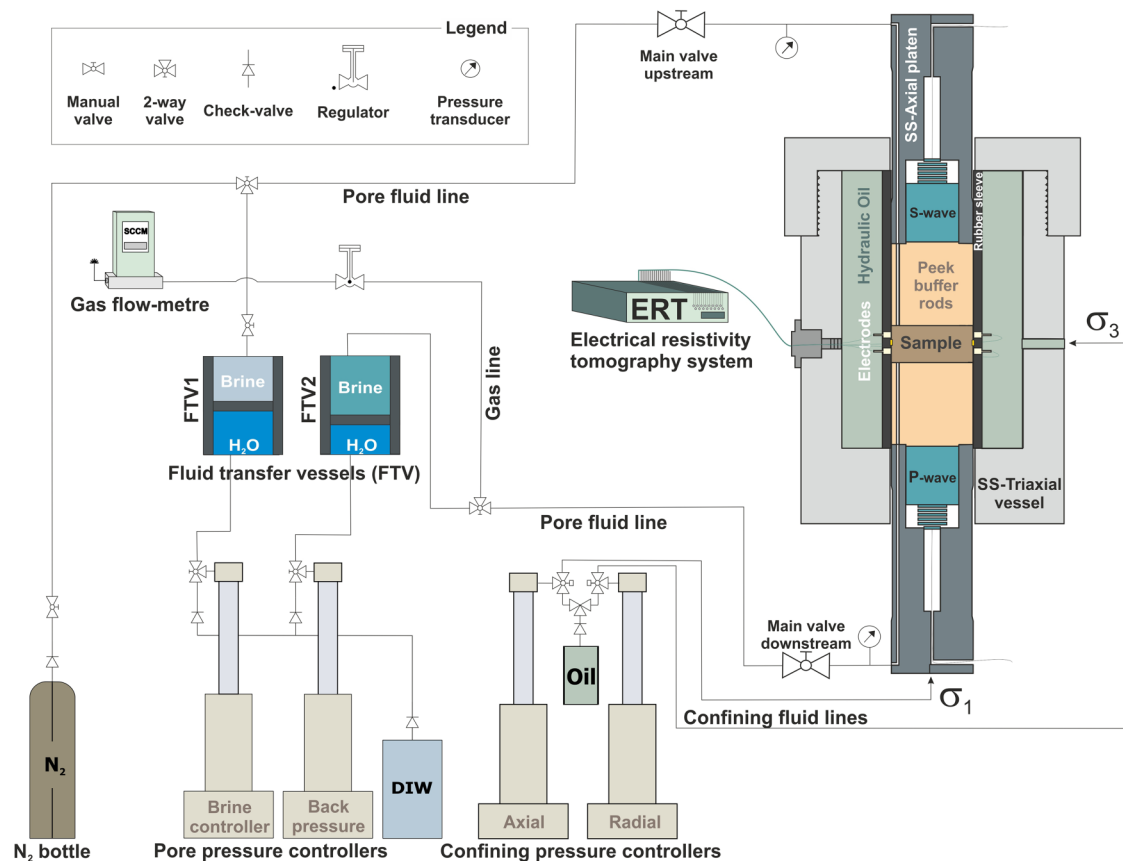


**FIGURE 1** Experimental setup for dry and single flow experiments at NOC Rock Physics Lab. The rig is assembled around a triaxial vessel with ultrasonic and electrical resistivity sensors, with automatic control (ISCO pumps) of pore and confining pressures. A gas flow-metre, a set of valves and two pressure transducers are allocated along the pipe-line to enable gas permeability measurements, together with geophysical measurements, at different stress conditions. The triaxial vessel is relatively scaled with respect to the sample size.

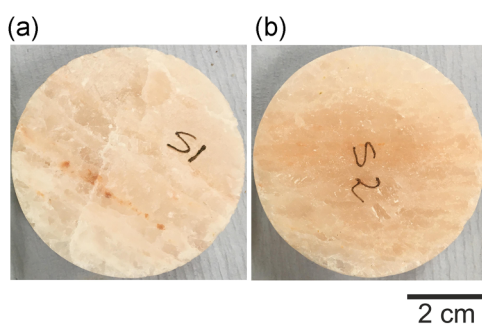


**FIGURE 2** Samples (a) S1 with visible cm-scale cracking, and (b) S2, apparently coherent.

selected for the dissolution tests. This  $P_c$  is a representative value for existing salt caverns for  $H_2$  storage around the world (HydrogenTCP-Task42, 2023); although this operational parameter might change if, as expected,  $H_2$  use increases. Once we reached the target  $P_c$ , the brine was delivered at a minimum  $P_p$  of 0.1 MPa. Then, keeping  $P_c$  constant,  $P_p$  was progressively increased (1 MPa stepwise) attempting at reaching a minimum effective pressure ( $P_e = P_c - P_p$ ) of

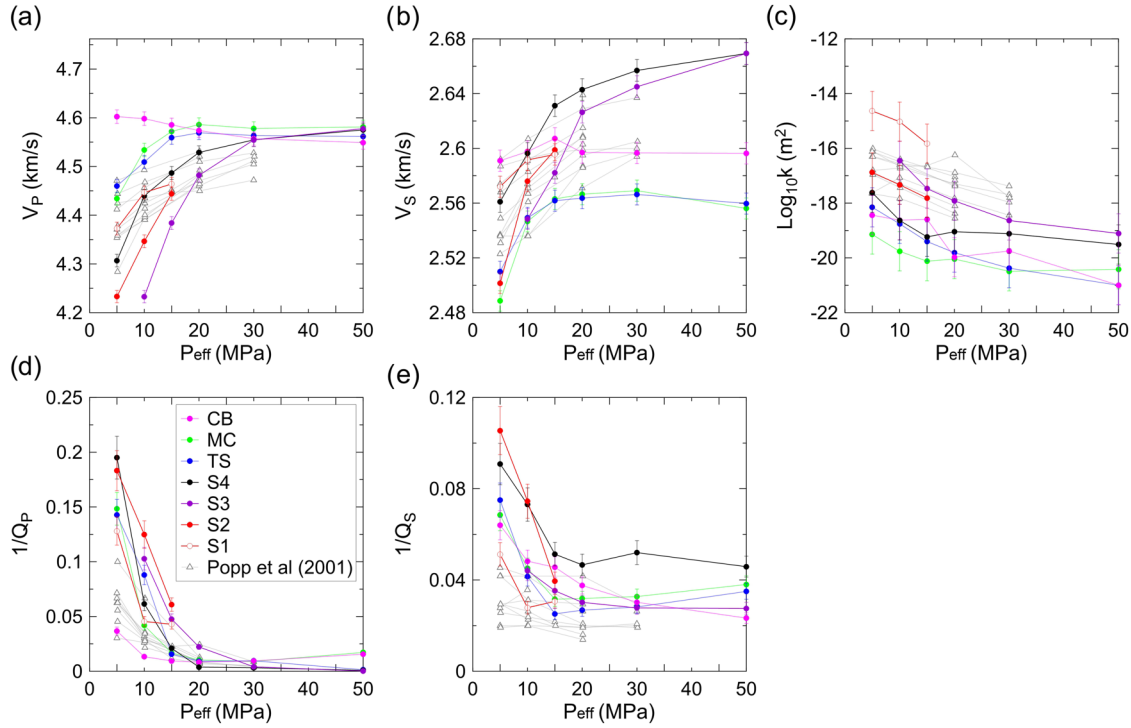
0.1 MPa. This procedure simulates a potential scenario of a progressive overpressure.

## HALITE ELASTIC AND TRANSPORT PROPERTIES

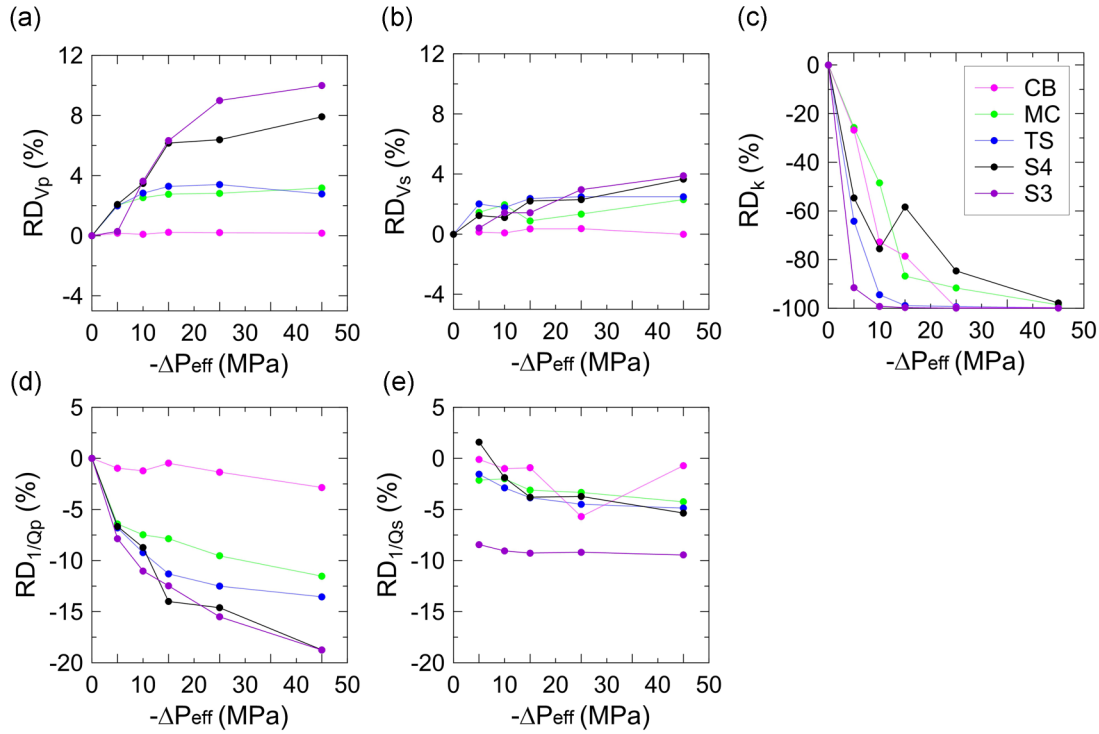
### Experimental results

Figure 3 shows our results during the loading steps (hysteresis is assessed separately; see Figure 4), together with Popp et al. (2001) data, as this is the most suitable dataset available in the literature to assess our results, both in terms of measured parameters and pressure conditions. Note that S1 and S2 were the samples used for the dissolution tests (see below) and therefore compressed (only) up to the target effective pressure planned for those tests (i.e.  $P_{eff} = 15$  MPa).

Overall, our elastic parameters and permeability agree with Popp et al. (2001)'s data (Figure 3).  $V_p$  varies between 4.2 and 4.6 km s<sup>-1</sup> (i.e. <10%) for the tested pressure range, increasing with effective pressure in all samples except for the CB sample, but all approaching to a common maximum



**FIGURE 3** (a–b) Ultrasonic wave velocities ( $V_p$  and  $V_s$ ), (d–e) attenuation factors ( $Q_p^{-1}$  and  $Q_s^{-1}$ ) and (c) permeability versus effective pressure for the (dry) halite samples used in this study (see Table 1; dataset available in Falcon-Suarez and Dale (2023)) and the data reported by Popp et al. (2001).



**FIGURE 4** Hysteresis effect on the ultrasonic wave velocities ( $V_p$  and  $V_s$ ), attenuation factors ( $Q_p^{-1}$  and  $Q_s^{-1}$ ) and permeability with respect to the increasing unloading, for the (dry) halite samples used in this study (see Table 1). The changes are expressed in terms of the relative difference  $RD = (Y - Y_0/Y_0) \times 100$ , with  $Y$  referring to any of the measured property and the subscript 0 to their initial value at 5 MPa.

( $\sim 4.6 \text{ km s}^{-1}$ ).  $V_S$  exhibits a similar range, between 2.5 and  $2.7 \text{ km s}^{-1}$  (i.e.  $< 7\%$ ), with a less defined maximum. The same occurs with their respective attenuation factors: Both  $Q_P^{-1}$  and  $Q_S^{-1}$  decrease towards zero with the increasing pressure, explained as a drop of energy dispersion related to microcracks closure.

Permeability spans nearly six orders of magnitude and decreases with increasing pressure in all samples. The permeability of our samples is all below Popp et al. (2001) except for sample S1 (Figure 3), which was specially selected for exhibiting cm-scale cracks (Figure 2). According to the elastic parameters and permeability results, the main changes in the halite rocks occur below 20 MPa. However, the lack of data in Popp et al. (2001) above 30 MPa hampers further analysis in this regard. Our results below 20 MPa also agree with the data reported by Zhang et al. (2020) for the permeability of halite under isotropic loading.

Figure 4 shows that all the parameters reflect a certain degree of hysteresis after compaction. In general, P- and S-wave velocities increase and the attenuations and permeability decrease with respect to their original (pre-load) values within the unloaded pressure range (i.e.  $-\Delta P_{\text{eff}}$ ) considered. S4 and S3 are the most affected samples, with up to 10% increase in  $V_P$  and 20% decrease in  $Q_P^{-1}$  after 50 MPa compaction, and 4% and 10% for  $V_S$  and  $Q_S^{-1}$ , respectively. This behaviour might be related to the shallower origin of these commercial samples, subjected for the first time to compaction. A similar degree of unrecovered permeability in all samples, particularly below 20 MPa (dropping between 60% and 100%), suggests similar permanent structural changes affecting the fluid pathways. Our results agree with the degree of hysteresis exhibited by the few samples subjected to unloading in Popp et al. (2001), both in terms of elastic properties and permeability, and with the degree of unrecovered permeability in Zhang et al. (2020).

## Combined assessment of elastic and transport data

During our tests, we have measured combined ultrasonic properties, permeability and porosity; the latter transport properties are more challenging to collect in the field (i.e. commonly based on well logging information, and therefore limited to the surroundings of the well). Cross-plotting permeability and elastic properties of halite rocks may therefore help to expand our interpretation of the transport properties of a target formation.

By cross-plotting our elastic and permeability results (Figure 5), we identify linear trends, which agree with the general fitting of Popp et al. (2001)'s data. The linearity is missing at high pressure ( $> 20 \text{ MPa}$ ) for permeability and the attenuation factors. This may indicate the existence of some

cracks (i.e. compliant porosity; Shapiro, 2003; Shapiro et al., 2015), but considering the low porosity of the samples, it could also be related to more complex grain-to-grain phenomena (e.g. inter-crystal boundaries responding to stress: boundaries between halite and non-halite minerals). Hence, in order to establish a more thorough assessment accounting for the pressure dependency of each variable, we analyse the potential of the following empirical relationship to explain our data:

$$Y(P_{\text{eff}}) = A_Y + B_Y P_{\text{eff}} - C_Y e^{-D_Y P_{\text{eff}}}, \quad (1)$$

with  $Y$  acting as any (usually elastic) rock property, and  $A$ ,  $B$ ,  $C$  and  $D$  being fitting parameters. These four fitting parameters describe:  $A$ , the crack-free value for the property  $Y$ ;  $B$ , the slope at high pressure;  $C$ , contribution of crack compliance on the property  $Y$  at zero effective pressure (Eberhart-Phillips et al., 1989), with  $A-C$ , expressing the zero-pressure velocity (Freund, 1992); and  $D$ , the rate of crack compliance with the increasing stress, a universal quantity based on sample elasticity, homogeneity and isotropic stress field, which has proved to be valid for sedimentary and crystalline (metamorphic) rocks of high and low porosity, and that also extends to transport (Kaselow & Shapiro, 2004).

This relationship has been successfully used to describe elastic properties of granular sedimentary rocks, including sandstones (e.g. Eberhart-Phillips et al., 1989; Zimmerman et al., 1986), siltstones and claystone (Freund, 1992) and transport properties in sandstones (e.g. Shapiro et al. (2015) for permeability; e.g. Kaselow and Shapiro (2004) and Falcon-Suarez et al. (2020) for electrical resistivity) with increasing  $P_{\text{eff}}$ . This relationship works well for sedimentary rocks under drained conditions as acoustic velocity increases with effective pressure as a result of pores and micro-cracks closure, which leads to reduced rock compressibility (Eberhart-Phillips et al., 1989). However, it has been also successfully used for low porosity/permeability rocks (e.g. Kaselow & Shapiro, 2004), which are expected to drain poorly due to low pore connectivity. Here we explore if this formula can also capture relations between elastic and transport properties at different  $P_{\text{eff}}$  for a ductile and crystalline rock such as halite. We use Equation (1) to obtain the four fitting parameters for our data and Popp et al. (2001), for  $V_P$ ,  $V_S$  and permeability. For permeability, we used  $Y = -\text{Log}_{10} k$  in Equation (1) to accommodate the fitting.

Figure 6 shows that the fitting parameters  $B$ ,  $C$  and  $D$  depend on the initial porosity for P- and S-wave velocities and permeability. The absence of further information about how porosity changes with pressure limits our interpretation of the fitting parameters of Equation (1), and therefore, we use linear adjustments to explain some of the observed correlations. For parameter  $A$ , elastic properties show a negligible dependency with porosity within the considered range (0%–7%), whereas

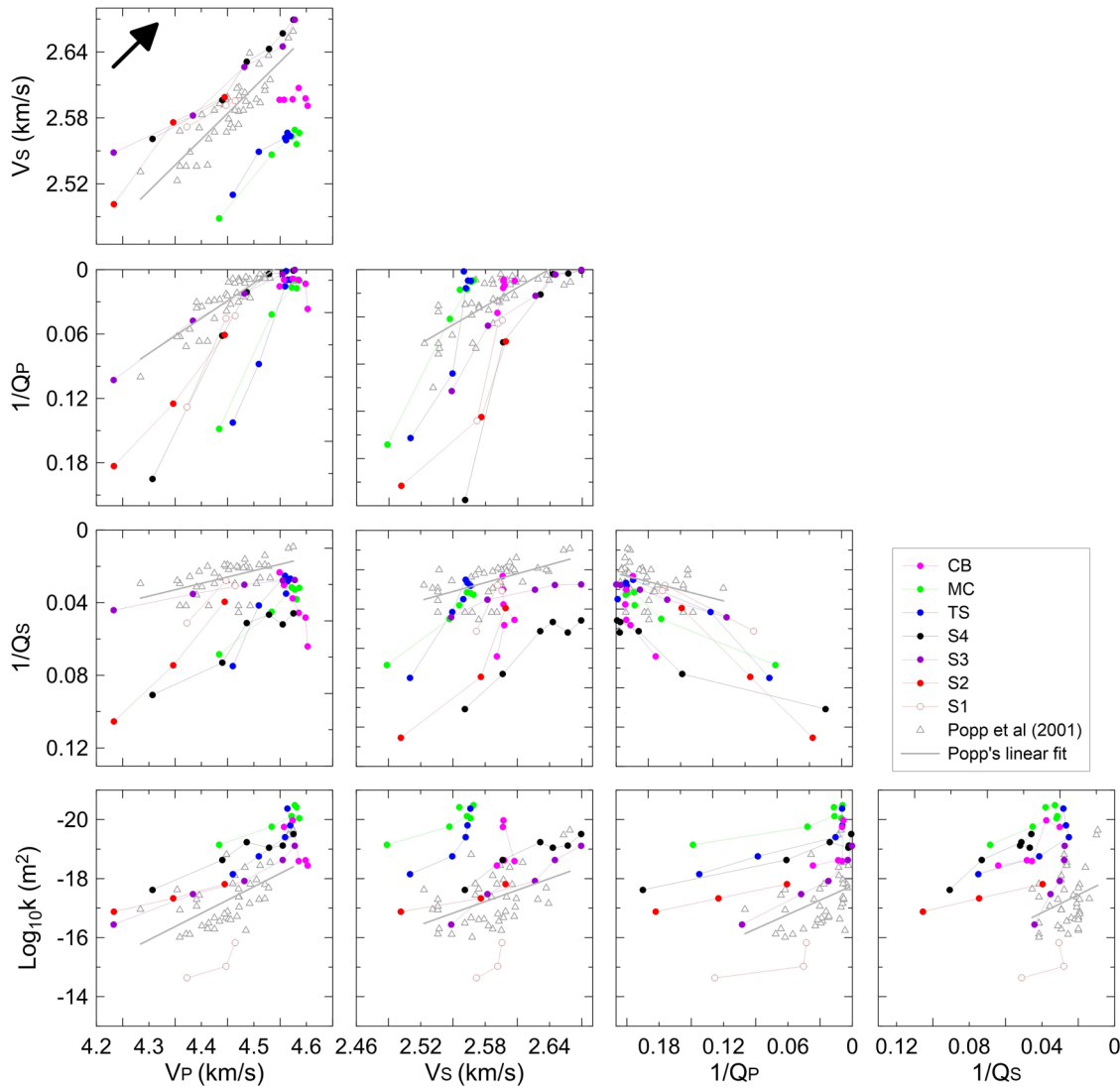


**FIGURE 5** Cross-plottings of ultrasonic wave velocities ( $V_p$  and  $V_s$ ), attenuation factors ( $Q_p^{-1}$  and  $Q_s^{-1}$ ) and permeability for the (dry) halite samples used in this study (Falcon-Suarez & Dale, 2023; see Table 1) and the data reported by Popp et al. (2001).  $P_{\text{eff}}$  is monotonically increasing according to the black arrow, in all cases.

a clearer positive correlation exists with permeability. This observation indicates that the velocity of the rock for such low porosities is mainly controlled by the velocity of the solid grains forming the skeleton (i.e. halite grain  $V_p$  is  $\sim 4.5 \text{ km s}^{-1}$  and  $V_s \sim 2.6 \text{ km s}^{-1}$ ). At high effective pressure (considered here to be above 20 MPa), the effective pressure seems to only affect permeability, as for the elastic properties the parameter  $B$  is close to zero – this is also illustrated in Figure 3 by the behaviour of  $V_p$  and  $V_s$  above 20 MPa. In the lower pressure domain, parameter  $C$  correlates differently with porosity for our data and Popp et al. (2001), both for the elastic properties and permeability (see dashed lines in Figure 6). This fact might be related to the way different minerals accommodate the discontinuities and the internal structure of the samples (i.e. crystal form linked back to primary deposition), as the main difference between the two datasets is the amount

and composition of the minerals accompanying the halite (i.e.  $<3\%$  dolomite in our samples;  $<9\%$  anhydrite in Popp et al. (2001)). The parameter  $D$  shows similar values for the ultrasonic waves and permeability, suggesting that both properties accommodate the compaction mechanisms similarly, but the higher  $C$  for permeability indicates that crack compliance has a stronger control in the changes of transport properties (Falcon-Suarez et al., 2020).

In terms of relationships between elastic and transport properties, Figure 7 shows that the fitting parameters for permeability correlate poorly with those of the  $V_p$ . These correlations should be treated as not statistically significant due to the reduced number of measurements per sample and the number of halite samples available for this study, and the lower limit of our experimental permeability-setup (i.e.  $10^{-21} \text{ m}^2$ ). Therefore, more samples and more precise sen-



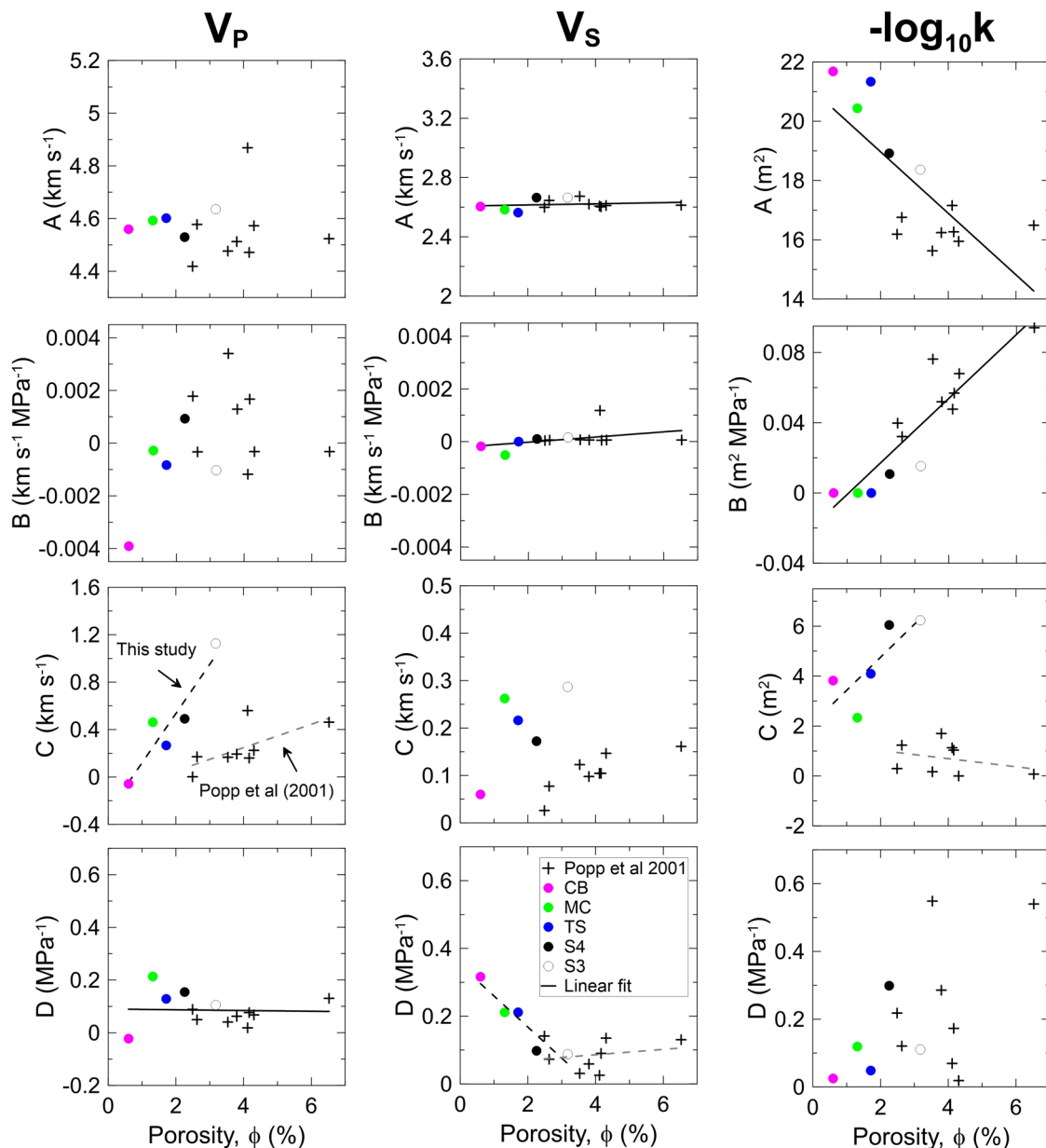


**FIGURE 6** Fitting parameters  $A$ ,  $B$ ,  $C$  and  $D$  of Equation (1) versus porosity for the ultrasonic wave velocities ( $V_p$  and  $V_s$ ) and permeability for the (dry) halite samples used in this study (Falcon-Suarez & Dale, 2023; see Table 1), and the data reported by Popp et al. (2001). Solid lines show linear fittings (where found) when all the points follow the same trend, while dashed for differing between the data of this study (black) and Popp et al. (2001) (grey).

sors are needed to accurately expand our interpretation to the realm of ultralow permeability ( $<10^{-21} \text{ m}^2$ ).

## CONTROLLED DISSOLUTION TESTS

The selected samples for the dissolution tests (i.e. S1 and S2) show similar elastic and transport values and trends than the rest of the tested samples (Figure 3). The main difference is the higher permeability of S1, based on visual observation of cm-scale cracks at the top and base of the sample that align

with the flow direction (Figure 2). As these cracks are also parallel to the direction of the wave propagation (i.e. perpendicular to the basal plane), the elastic properties, including the attenuation factors, remain unaffected (e.g. Falcon-Suarez et al., 2020).

The dissolution test on sample S1 lasted  $\sim 4$  h (Figure 8). The test was terminated as a result of an early rock dissolution event that commenced nearby the inlet pore fluid port and quickly propagated peripheral around the outer part of the sample, triggering the failure of the inner rubber sleeve in the triaxial vessel. The little time window of this test shows incon-

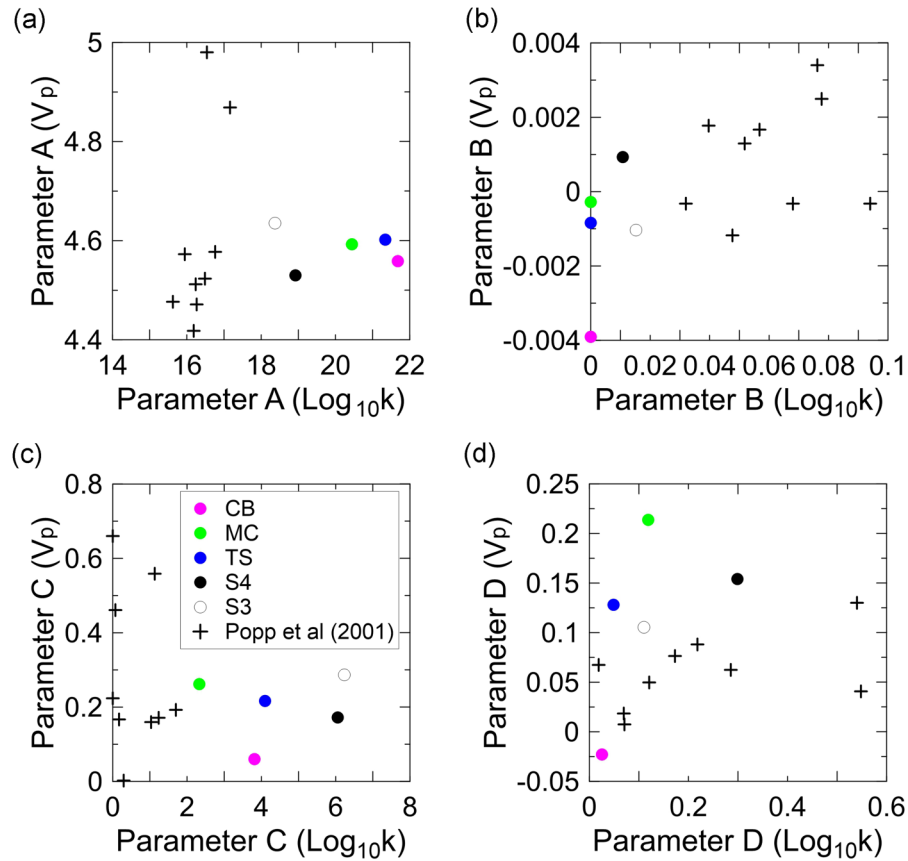


**FIGURE 7** (a–d) Fitting parameters  $A$ ,  $B$ ,  $C$  and  $D$  of Equation (1) of the ultrasonic P-wave velocity ( $V_p$ ) versus the permeability ones, for the halite samples used in this study (Falcon-Suarez & Dale, 2023; see Table 1) and the data reported by Popp et al. (2001).

clusive trends of the elastic properties with a slight increase in  $V_p$  and  $Q_p^{-1}$ , possibly due to increasing saturation of the central part of the sample via (fast) imbibition, whereas the minor increase in  $V_s$  might be related to crack closure in localized areas. Resistivity was unable to be collected because of some electrode-rock missing contacts associated with the early lateral dissolution. This early dissolution is fairly consistent with Davies (1989) who suggested that the dissolution of halite in contact with unsaturated brine is ‘essentially instantaneous’, irrespective of the rate. Our experimental results also agree with Weisbrod et al. (2012) hypothesis of fast dissolution channels formation along preferential fluid pathways in areas of minimum resistance to flow, such as cracks, even under high effective pressure (i.e. 15 MPa).

The dissolution test on the intact halite sample S2 (Figure 9) shows that the geophysical parameters vary very little during the first  $P_{eff}$  step, when the sample was exposed to brine under minimum pore pressure ( $P_p = 0.1$  MPa, i.e. maximum  $P_{eff} = 15$  MPa) for over 3 days (see the difference between interlude periods and effective time in Figure 9). During this period, we assume that the sample is only partially saturated in brine, as  $Q_p^{-1}$  exhibits a little prompt increase in agreement with theoretical  $Q_p^{-1}$ -saturation curves with very small gas patchy areas at high (>60%) water saturation (Amalokwu

et al., 2014), and resistivity starts decreasing after the first increment in pore pressure. Then,  $V_p$  and  $V_s$  progressively increase with the increasing  $P_p$  (despite the decrease in  $P_{eff}$ ). Halite dissolution increases both the porosity and brine content in the sample. Hence, the observed increase in elastic velocities can be explained by a dissolution phase in which the increase in porosity and brine generates a greater decrease in the bulk density than in the elastic moduli. The brine saturation is heterogeneously distributed in the sample, more localized in the surroundings of the pore fluid inlet port, as interpreted from the decrease of resistivity in that area (electrical resistivity tomography [ERT]-3, Figure 10).  $V_p$  commences to decrease when  $P_{eff}$  is  $\sim 6$  MPa, whereas  $V_s$  slightly increases. Here, dissolution generates a decrease in density (i.e. increase in porosity and brine replacing halite) that is lower than the combined decrease in bulk and shear moduli (so  $V_p$  decreases), but higher than the decrease in shear modulus (this trend is more significant with the decreasing  $P_{eff}$ ). At this point, resistivity drops by  $\sim 50\%$  but still shows a highly heterogeneous distribution in the sample (ERT-4, Figure 10). This evolution has a complex interpretation, which lies in the interplay of both fracturing and dissolution. Once  $P_{eff}$  reaches its minimum (i.e.  $P_{eff} = 0.1$  MPa), the test continues during 2 more days without significant changes

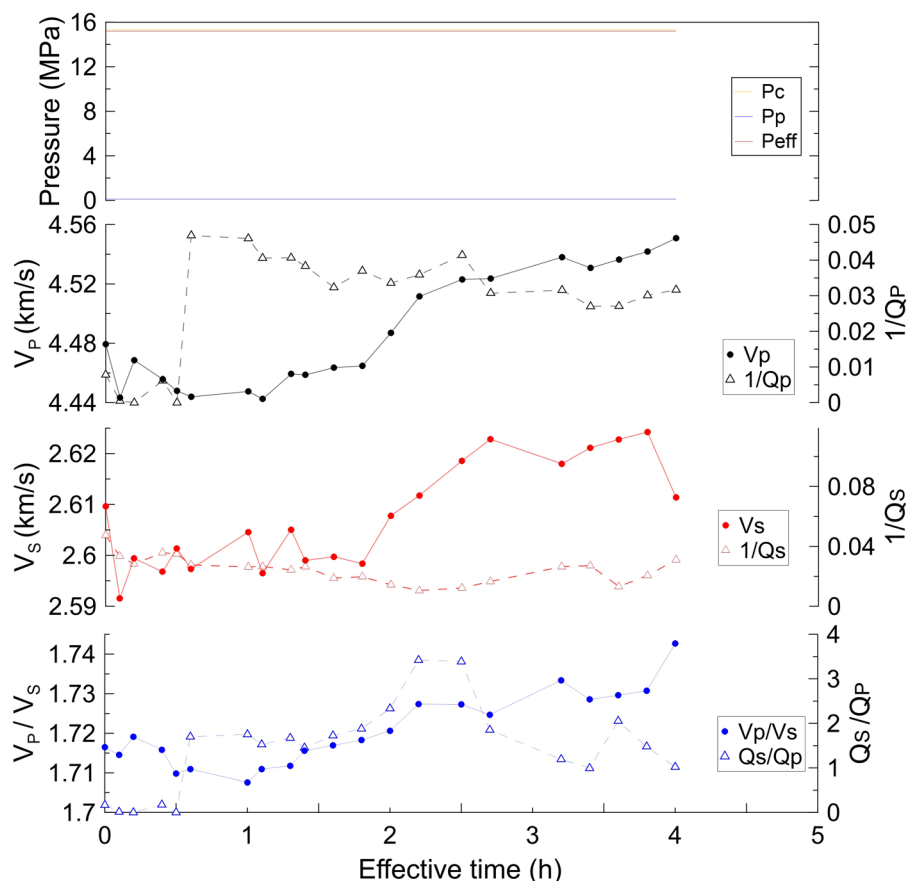


**FIGURE 8** Dissolution test on the halite sample S1 (Falcon-Suarez & Dale, 2023). Ultrasonic wave velocities ( $V_p$  and  $V_s$ ), attenuation factors ( $Q_p^{-1}$  and  $Q_s^{-1}$ ) and  $V_p/V_s$  ratio versus effective time (i.e. disregarding interludes with no measurements).

in any of the geophysical properties (i.e.  $V_p \sim 4.5 \text{ km s}^{-1}$ ,  $V_s \sim 2.6 \text{ km s}^{-1}$  and resistivity  $\sim 30 \text{ } \Omega \text{ m}$ ). From ERT-5 to ERT-6 (Figure 10), the inlet area exhibits a large decrease in resistivity, suggesting that dissolution was occurring preferentially during the period of minimum  $P_{\text{eff}}$ . From our resistivity tomography data, we interpret the initiation of the channelling in sample S2 at  $P_{\text{eff}} \leq 3 \text{ MPa}$  (Figure 10).

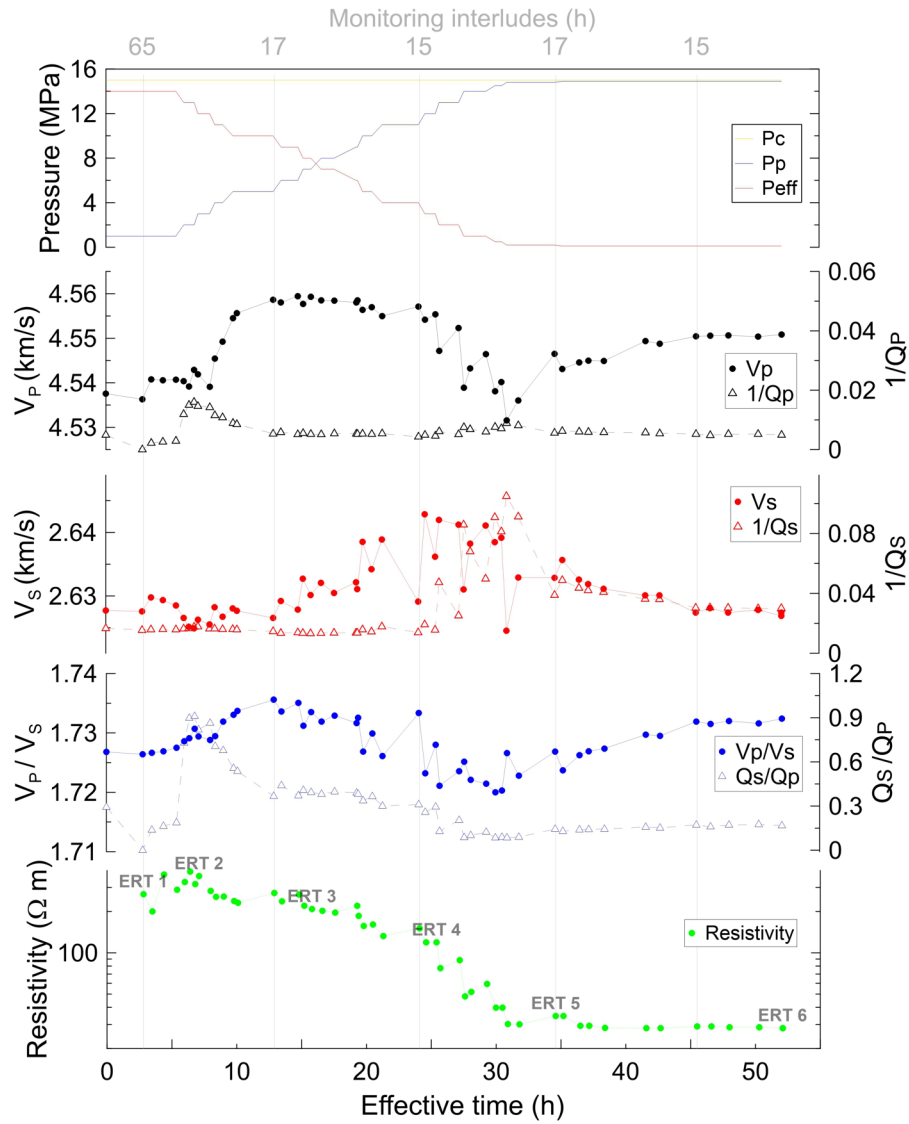
To properly interpret the dissolution test, we need to understand the actual reach of our geophysical measurements. Figure 11a shows the configuration of our geophysical sensors in the vessel. The incidence of the P- and S-waves limits the interpretation of our experimental data to the 38 mm diameter of the central area of our samples. By the contrary, the lateral position of the electrodes provides a bulk electrical resistivity record of the whole sample. Therefore, unlike resistivity, our ultrasonic sensors are unable to measure the changes occurring in the outer areas of the samples.

Figure 11b shows that dissolution on S1 (fractured sample) developed a peripheral channel from the inlet port – rock contact. The channelling progressed horizontally, instead of following the visual (pseudo-) vertical fracturing network (Figure 11b.1), suggesting a 3D cubic cracking network (completed by a third fracture family parallel to the basal plane) in

agreement with the cleavage planes observed by Popp et al. (2001). The basal plane could have developed as a result of the early dissolution and fracturing, as the attenuation data versus pressure (Figure 3) suggested the absence of fractures perpendicular to the wave propagation. S3 post-testing shows a smaller dissolution volume near the inlet port (Figure 11c), as previously observed in the ERT (Figure 10). In this case, the absence of initial fracturing led to localized dissolution near the inlet, with slow diffusion backwards into the pipe system. The post-test drying suggests a total salt dissolution volume of  $\sim 6\%$  during the S2 test, whereas over 25% for S1, although, in the latter case, this is just a rough estimate due to the sample was oil-contaminated (which is only partially removable by oven-drying) during the failure of the experimental setup.

## DISCUSSION

Operating and future sites for underground hydrogen storage (UHS) in salt caverns are commonly placed at depths (up to 2000 m) that can lead to confining pressures above 20 MPa (Caglayan et al., 2020; Crotogino et al., 2018; Cyran, 2020; Zivar et al., 2020). However, the energy transition challenge



**FIGURE 9** Dissolution test on the halite sample S2 (Falcon-Suarez & Dale, 2023). Ultrasonic wave velocities ( $V_p$  and  $V_s$ ), attenuation factors ( $Q_p^{-1}$  and  $Q_s^{-1}$ ),  $V_p/V_s$  ratio and electrical resistivity versus effective time (i.e. disregarding interludes with no measurements), for a decreasing effective pressure ( $P_{eff}$ ) sequence. Electrical resistivity tomography was computed six times (ERT 1–6) during the test (Falcon-Suarez & Dale, 2023).

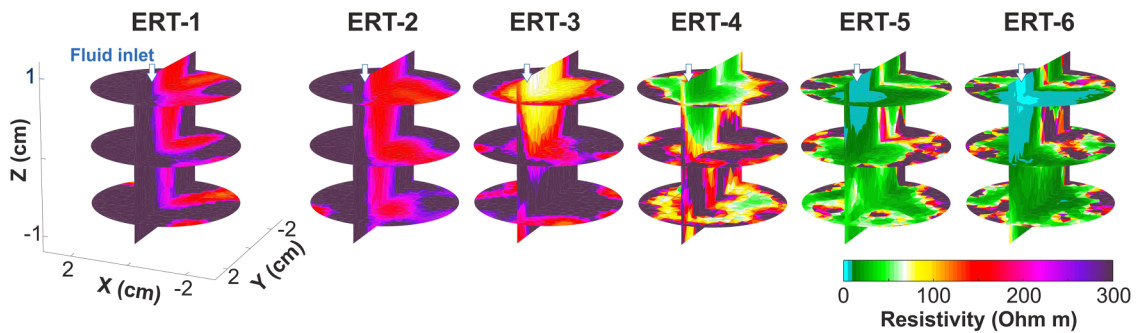


**FIGURE 10** Electrical resistivity tomography (ERT) computed during the dissolution test on the halite sample S2 (see Figure 9).



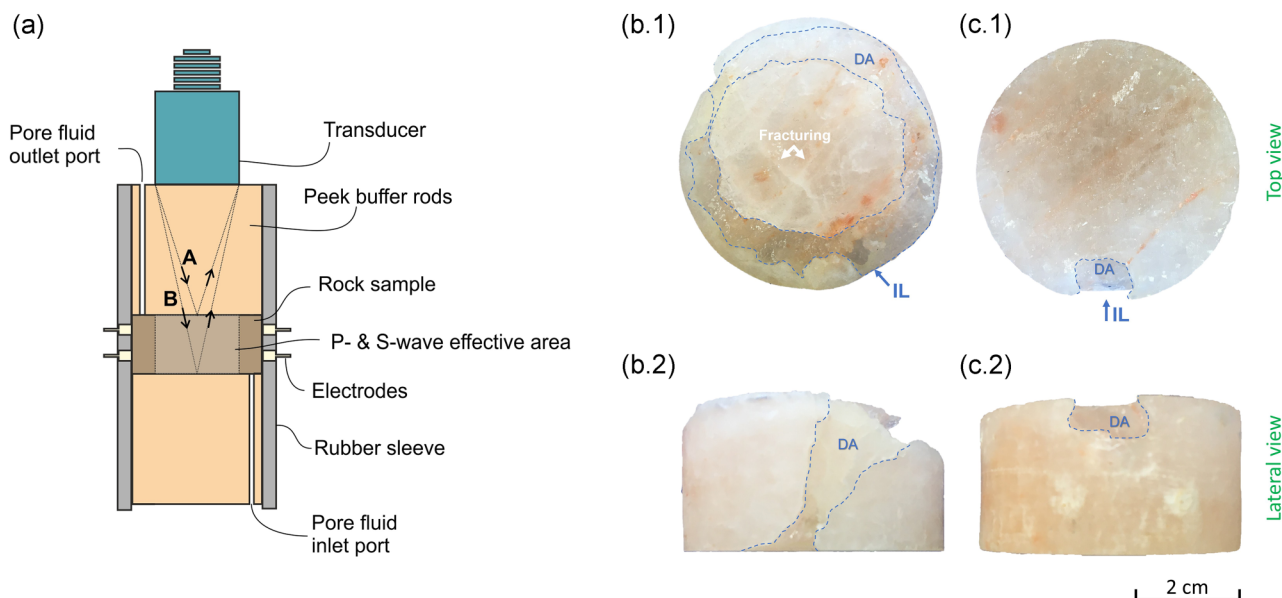


**FIGURE 11** (a) Configuration of the geophysical sensors around the rock sample in the experimental rig (Figure 1). Top (1) and lateral (2) view of samples (b) S4 and (c) S3 post-testing.

will require refined storage strategies, aiming to combine CO<sub>2</sub> sequestration and, for instance, H<sub>2</sub> storage in the same area to enhance the effectivity of the whole process (Akhurst et al., 2021). This could lead to shallower UHS to enable the more compressible CO<sub>2</sub> to be stored in deeper reservoirs underneath.

We have identified a turning point in the compaction trend around 15–20 MPa in our experimental data. All the measured properties change faster with effective pressure below 20 MPa (Figure 3) but inelastically, as interpreted from the high hysteresis carried by all the parameters in all samples below this pressure (Figure 4). This finding is relevant for UHS as seasonal energy demands will generate cyclic changes in  $P_{\text{eff}}$  and changes in salt rock behaviour. According to our results, periods with effective pressures above 20 MPa (e.g. winter; depleted reservoir due to high energy demand) will lead to a safer state of the underground compartment, by enhancing the sealing (i.e. lowering permeability) and the mechanical properties of the rock (at least up to 50 MPa), as inferred from the  $V_P$  and  $V_S$  increase and  $Q_P^{-1}$  and  $Q_S^{-1}$  decrease towards asymptotic values (i.e. rock quality tends to increase with  $P_{\text{eff}}$  – effective cracks closure). Periods of lower  $P_{\text{eff}}$  (e.g. summer periods; larger volumes of H<sub>2</sub> stored due to low energy demand) would have negligible effect on cavern behaviour.

The results collected in this study agree with the limited data available in the literature for elastic and transport properties and their pressure dependency of halite rocks. The suitability of the dataset reported by Popp et al. (2001) contrasts with the low-pressure range (<30 MPa) and number of measurements collected per sample. This fact hampers the statistical significance during data analysis and partly

limits the generalization of our correlations between elastic waves and permeability. Our assessment of elastic waves changes with effective pressure shows a good correlation between  $V_P$  and  $V_S$ , and so the  $V_P/V_S$  ratio with effective pressure. This result is particularly interesting for offshore exploration surveys, where the shear (S-) wave collection is limited by the commonly encountered low amplitude of S-waves in marine wide-angle seismic data (e.g. Niu et al., 2022). Furthermore, where S-wave is available, changes in the pressure dependency  $V_P$ – $V_S$  correlation could serve as an indicator of partial saturation, as this will affect the bulk compressibility of the rock and therefore the shape of the loading curve. This possibility would be of great interest to interpret leaks from borehole infrastructure associated with storage caverns through overburden formations from 4D seismic imaging (Robinson et al., 2021). However, to further analyse this possibility in halite rocks, we need to collect more experimental data under both dry and fully saturated conditions and establish a more statistical sound dataset.

The dissolution tests on samples S1 (fractured) and S2 (intact) demonstrate that even small structural discontinuities may significantly impact the dissolution patterns, in agreement with the key finding of the halite dissolution experiment conducted by Field et al. (2019). Weisbrod et al. (2012) focused on the dissolution patterns of salt rock when an unsaturated solution with respect to halite flowed through the salt cores. They found that dissolution patterns are related to rock structural, mineralogic and petrographic heterogeneities (preferential dissolution pathways in areas with cracks; larger surface areas enhance dissolution), flow rate and gravity. But the flow rate only affects the dissolution pattern if an outlet

for fluid escape exists – one basic requirement for dissolution to happen (Johnson, 2005). Our results suggest that the presence of discontinuities likely dominates dissolution, particularly when they are aligned (and in contact) with the fluid flow. Even an uncontrolled increase in fluid pressure (e.g. as a result of constant flow through intact salt rocks during caverning) seems to lead to minor changes than those expected in a fractured rock with a minimum fluid pressure. In a large scale, the dissolution of halite free of fractures would lead to low salt-removal rates and lead to more ductile subsidence than fractured formations, which with higher salt-removal rates may generate brittle subsidence with associated vertical fracturing (Davies, 1989). Worth mentioning is that no subsidence cases have been reported so far from modern-day engineered caverns, and only minor mine subsidence associated with halite formations currently considered for energy storage (e.g. Teesside; Cooper, 2020).

The presence of structural discontinuities and heterogeneities (e.g. shape, orientations and composition of insoluble lithologies, halite fabric and stress-related microstructural changes; Field et al., 2019) influences largely the safety and placement of salt caverns that may be used for UHS activities (Cyran, 2020; Duffy et al., 2023). We have observed how vertical discontinuities that control fluid migration (dispersion or channelling) may be undetectable from acoustic P- and S-wave attributes (i.e. velocities and attenuation factors). This finding has important implications for UHS in salt formations, as the existence of seismically unseen vertical fractures might lead to undesirable dissolution events around the borehole infrastructure during caverning. This might also impact the monitoring resolution during caverning in salt domes where the preferred cavern shape is a vertical cylinder with low horizontal-to-vertical ratio, unlike the caverns in bedded salt deposits (Cyran, 2020). One strategy could be complementing the conventional 3D seismic data with higher resolution multi-frequency surveys (Robinson et al., 2021). Our results suggest that electrical resistivity might also contribute to the monitoring of the caverning process due to the contrast between the rock and the fluid in the pores/cavern. Although our dissolution test on the intact halite sample clearly shows the evolution of the aperture nearby the sample inlet (Figure 10), these results should be carefully interpreted, as we commenced the test from a high resistivity (dry sample) stage. This circumstance amplifies the electrical contrast between rock and pore fluid. However, by the end of the test (ERT 5 and 6), when the rock is partially saturated, it still shows a large contrast (by  $\sim 50 \Omega \text{ m}$ ) between frame and pores. Nevertheless, the detection of subvertical fractures from electromagnetic surveys would be conditioned by the inherent low spatial resolution of the method (Gehrmann et al., 2021), which would limit the interpretation of the actual fracture size (i.e. length and aperture).

## CONCLUSIONS

Seismic and electromagnetic sources can be used for monitoring changes in mechanical and fluid flow properties of the salt formations, during both the caverning development and operational hydrogen storage/extraction activities.

Elastic properties and permeability are linearly correlated up to 20 MPa effective pressure; this information can be used for underground hydrogen storage reservoir selection. Effective pressures above 20 MPa will lead to a safer state of the underground compartment, by enhancing the sealing (i.e. lowering permeability) and the mechanical properties of the rock. However, an extended database covering more samples and using more precise sensors is needed to extrapolate these elastic-transport relationships to permeabilities below  $10^{-21} \text{ m}^2$ .

Rock heterogeneities likely dominate the dissolution in halite formations, with even small structural discontinuities playing a significant impact on dissolution patterns.

## ACKNOWLEDGEMENTS


The experiment was conducted at the NOC Rock Physics Laboratory in Southampton. We would like to thank Dr Audrie Ougier-Simonin and Dr Edward Hough (British Geological Survey) for their valuable comments on the manuscript.

## DATA AVAILABILITY STATEMENT

The data that support the findings of this study are openly available in the U.K. National Geoscience Data Centre (NGDC) repository at <https://doi.org/10.5285/13c05fe8-0d1d-49e5-b55e-5cf4ef241c70>.

## ORCID

Ismael Himar Falcon-Suarez  <https://orcid.org/0000-0001-8576-5165>

Hector Marin-Moreno  <https://orcid.org/0000-0002-3412-1359>

## REFERENCES

- Akhurst, M., Pearce, J., Sunny, N., Shah, N., Goldthorpe, W. & Avignon, L. (2021) Tools and options for hydrogen and CCS cluster development and acceleration—UK case study, ELEGANCY project. In: Proceedings of the 15th Greenhouse Gas Control Technologies Conference. Available from: <https://doi.org/10.2139/ssrn.3815268>
- Amalokwu, K., Best, A.I., Sothcott, J., Chapman, M., Minshall, T. & Li, X.-Y. (2014) Water saturation effects on elastic wave attenuation in porous rocks with aligned fractures. *Geophysical Journal International*, 197, 943–947. Available from: <https://doi.org/10.1093/gji/ggu076>
- Anderson, R.Y. & Kirkland, D.W. (1980) Dissolution of salt deposits by brine density flow. *Geology*, 8, 66–69. Available from: [https://doi.org/10.1130/0091-7613\(1980\)8\(66:dosdbb\)2.0.co;2](https://doi.org/10.1130/0091-7613(1980)8(66:dosdbb)2.0.co;2)
- Beauheim, R.L. & Roberts, R.M. (2002) Hydrology and hydraulic properties of a bedded evaporite formation. *Journal of Hydrology*,

- 259, 66–88. Available from: [https://doi.org/10.1016/S0022-1694\(01\)00586-8](https://doi.org/10.1016/S0022-1694(01)00586-8).
- Beauheim, R.L., Saulnier, G.J., Jr. & Avis, J.D. (1991) *Interpretation of brine-permeability tests of the Salado Formation at the Waste Isolation Pilot Plant site: first interim report*. United States. Available from: <https://doi.org/10.2139/ssrn.3815268>
- Best, A.I. (1992) The prediction of the reservoir properties of sedimentary rocks from seismic measurements. Ph.D. thesis, Reading: University of Reading.
- Brodsky, N.S. (1994) *Hydrostatic and shear consolidation tests with permeability measurements on Waste Isolation Pilot Plant crushed salt*. Report number: SAND-93-7058, United States. Available from: <https://doi.org/10.2139/ssrn.3815268>
- Caglayan, D.G., Weber, N., Heinrichs, H.U., Linßen, J., Robinius, M., Kukla, P.A. et al. (2020) Technical potential of salt caverns for hydrogen storage in Europe. *International Journal of Hydrogen Energy*, 45, 6793–6805. Available from: <https://doi.org/10.1016/j.ijhydene.2019.12.161>
- Cooper, A.H. (2002) Halite karst geohazards (natural and man-made) in the United Kingdom. *Environmental Geology*, 42, 505–512. Available from: <https://doi.org/10.1007/s00254-001-0512-9>
- Cooper, A.H. (2020) Geological hazards from salt mining, brine extraction and natural salt dissolution in the UK. In: *Geological Society, London, Engineering Geology Special Publications*, 29, pp. 369–387. Available from: <https://doi.org/10.1144/EGSP29.14>
- Cosenza, P. & Ghoreychi, M. (1997) Permeability evolution of rock salt under mechano-chemical stresses. *Bulletin de la Societe Geologique de France*, 168, 313–324.
- Crotogino, F., Schneider, G.-S. & Evans, D.J. (2018) Renewable energy storage in geological formations. *Proceedings of the Institution of Mechanical Engineers, Part A: Journal of Power and Energy*, 232, 100–114. Available from: <https://doi.org/10.1177/0957650917731181>
- Cyran, K. (2020) Insight into a shape of salt storage caverns. *Archives of Mining Sciences*, 65, 363–398. Available from: <https://doi.org/10.24425/ams.2020.133198>
- Dale, M.S., Falcon-Suarez, I.H. & Marín-Moreno, H. (2021) Geophysical response to dissolution of undisturbed and fractured evaporite rock during brine flow. In: EGU General Assembly 2021. Available from: <https://doi.org/10.5194/egusphere-egu21-15572>
- Dale, M.S., Marín-Moreno, H., Falcon-Suarez, I.H., Grattoni, C., Bull, J.M. & McNeill, L.C. (2021) The Messinian Salinity Crisis as a trigger for high pore pressure development in the Western Mediterranean. *Basin Research*, 33, 2202–2228. Available from: <https://doi.org/10.1111/bre.12554>
- Davies, P.B. (1989) Assessing deep-seated dissolution-subsidence hazards at radioactive-waste repository sites in bedded salt. *Engineering Geology*, 27, 467–487. Available from: [https://doi.org/10.1016/0013-7952\(89\)90042-2](https://doi.org/10.1016/0013-7952(89)90042-2)
- Duffy, O., Hudec, M., Peel, F., Apps, G., Bump, A., Moscardelli, L. et al. (2023) The role of salt tectonics in the energy transition: an overview and future challenges. *Tektonika*, 1, 18–48. Available from: <https://doi.org/10.55575/tektonika2023.1.1.11>
- Eberhart-Phillips, D., Han, D.-H. & Zoback, M.D. (1989) Empirical relationships among seismic velocity, effective pressure, porosity, and clay content in sandstone. *Geophysics*, 54, 82–89. Available from: <https://doi.org/10.1190/1.1442580>
- Ezersky, M. & Goretsky, I. (2014) Velocity–resistivity versus porosity–permeability inter-relations in Dead Sea salt samples. *Engineering Geology*, 183, 96–115. Available from: <https://doi.org/10.1016/j.enggeo.2014.09.009>
- Falcon-Suarez, I.H. & Dale, M. (2023) Geophysical and transport properties of salt rocks subjected to loading/unloading, and during dissolution. NERC EDS National Geoscience Data Centre (dataset). Available from: <https://doi.org/10.5285/13c05fe8-0d1d-49e5-b55e-5cf4ef241c70>
- Falcon-Suarez, I., Bayrakci, G., Minshull, T.A., North, L.J., Best, A.I., Rouméjon, S. et al. (2017) Elastic and electrical properties and permeability of serpentinites from Atlantis Massif, Mid-Atlantic Ridge. *Geophysical Journal International*, 211, 708–721. Available from: <https://doi.org/10.1093/gji/ggx341>
- Falcon-Suarez, I.H., North, L., Callow, B., Bayrakci, G., Bull, J. & Best, A. (2020) Experimental assessment of the stress-sensitivity of combined elastic and electrical anisotropy in shallow reservoir sandstones. *Geophysics*, 85, MR271. Available from: <https://doi.org/10.1190/geo2019-0612.1>
- Field, L.P., Milodowski, A.E., Evans, D., Palumbo-Roe, B., Hall, M.R., Marriott, A.L. et al. (2019) Determining constraints imposed by salt fabrics on the morphology of solution-mined energy storage cavities, through dissolution experiments using brine and seawater in halite. *Quarterly Journal of Engineering Geology and Hydrogeology*, 52, 240–254. Available from: <https://doi.org/10.6084/m9.figshare.c.4282454>
- Fokker, P.A. (1995) The behaviour of salt and salt caverns. PhD thesis, Delft University of Technology
- Freund, D. (1992) Ultrasonic compressional and shear velocities in dry clastic rocks as a function of porosity, clay content, and confining pressure. *Geophysical Journal International*, 108, 125–135. Available from: <https://doi.org/10.1111/j.1365-246X.1992.tb00843.x>
- Gehrmann, R.S., Provenzano, G., Böttner, C., Marín-Moreno, H., Bayrakci, G., Tan, Y.Y. et al. (2021) Porosity and free gas estimates from controlled source electromagnetic data at the Scanner Pockmark in the North Sea. *International Journal of Greenhouse Gas Control*, 109, 103343. Available from: <https://doi.org/10.1016/j.ijggc.2021.103343>
- Gloyna, E.F. & Reynolds, T.D. (1961) Permeability measurements of rock salt. *Journal of Geophysical Research (1896-1977)*, 66, 3913–3921. Available from: <https://doi.org/10.1029/JZ066i011p03913>
- Hydrogentcp-Task42. (2023) In: Hegen, D. (Ed.) Underground hydrogen storage: technology monitor report. Hydrogentcp-Task42. Online.
- Jiang, D., Li, Z., Liu, W., Ban, F., Chen, J., Wang, Y. et al. (2021) Construction simulating and controlling of the two-well-vertical (TWV) salt caverns with gas blanket. *Journal of Natural Gas Science and Engineering*, 96, 104291. Available from: <https://doi.org/10.1016/j.jngse.2021.104291>
- Johnson, K. (1989) Development of the Wink Sink in west Texas, USA, due to salt dissolution and collapse. *Environmental Geology and Water Sciences*, 14, 81–92. Available from: <https://doi.org/10.1007/BF01728499>
- Johnson, K. (2005) Subsidence hazards due to evaporite dissolution in the United States. *Environmental Geology*, 48, 395–409. Available from: <https://doi.org/10.1007/s00254-005-1283-5>
- Kaselow, A. & Shapiro, S.A. (2004) Stress sensitivity of elastic moduli and electrical resistivity in porous rocks. *Journal of Geophysics and Engineering*, 1, 1–11. Available from: <https://doi.org/10.1088/1742-2132/1/1/001>



- Klinkenberg, L.J. (1941) *The permeability of porous media to liquids and gases. Drilling and production practice*. New York, NY: American Petroleum Institute.
- Kröhn, K.-P., Zhang, C.-L., Czaikowski, O., Stührenberg, D. & Heemann, U. (2015) The compaction behaviour of salt backfill as a THM-process. In: *Mechanical behaviour of salt VIII*: CRC Press, pp. 49–60. Available from: <https://doi.org/10.1201/b18393-8>
- Li, J., Shi, X. & Zhang, S. (2020) Construction modeling and parameter optimization of multi-step horizontal energy storage salt caverns. *Energy*, 203, 117840. Available from: <https://doi.org/10.1016/j.energy.2020.117840>
- Liu, X., Yang, X., Zhong, Z., Liang, N., Wang, J. & Huang, M. (2015) Research on dynamic dissolving model and experiment for rock salt under different flow conditions. *Advances in Materials Science and Engineering*, 2015, 959726. Available from: <https://doi.org/10.1155/2015/959726>
- Lugli, S., Schreiber, B.C. & Triberti, B. (1999) Giant polygons in the Realmonte Mine (Agrigento, Sicily); evidence for the desiccation of a Messinian halite basin. *Journal of Sedimentary Research*, 69, 764–771. Available from: <https://doi.org/10.2110/jsr.69.764>
- Mavko, G., Mukerji, T. & Dvorkin, J. (2009) *Rock physics handbook—tools for seismic analysis in porous media*. New York: Cambridge University Press.
- Mccann, C. & Sothcott, J. (1992) Laboratory measurements of the seismic properties of sedimentary rocks. *Geological Society, London, Special Publications*, 65, 285–297. Available from: <https://doi.org/10.1144/gsl.sp.1992.065.01.22>
- Metwally, Y.M. & Sondergeld, C.H. (2011) Measuring low permeabilities of gas-sands and shales using a pressure transmission technique. *International Journal of Rock Mechanics and Mining Sciences*, 48, 1135–1144. Available from: <https://doi.org/10.1016/j.ijrmms.2011.08.004>
- Niu, X., Minshull, T.A., Li, J., Ruan, A., Wu, Z., Wei, X. et al. (2022) Shear wave velocity structure and crustal lithology beneath the ultra-slow spreading Southwest Indian Ridge at 50°E. *Geophysical Journal International*, 233, 1416–1428. Available from: <https://doi.org/10.1093/gji/ggac516>
- North, L.J. & Best, A.I. (2014) Anomalous electrical resistivity anisotropy in clean reservoir sandstones. *Geophysical Prospecting*, 62, 1315–1326. Available from: <https://doi.org/10.1111/1365-2478.12183>
- North, L., Best, A.I., Sothcott, J. & Macgregor, L. (2013) Laboratory determination of the full electrical resistivity tensor of heterogeneous carbonate rocks at elevated pressures. *Geophysical Prospecting*, 61, 458–470. Available from: <https://doi.org/10.1111/j.1365-2478.2012.01113.x>
- Pfeifle, T.W. & Hurtado, L.D. (1998) Permeability of natural rock salt from the Waste Isolation Pilot Plant (WIPP) during damage evolution and healing. In: North American Rock Mechanics Society conference, Cancun, Mexico. Available from: <https://www.osti.gov/biblio/650135>
- Popp, T. & Kern, H. (1998) Ultrasonic wave velocities, gas permeability and porosity in natural and granular rock salt. *Physics and Chemistry of the Earth*, 23, 373–378. Available from: [https://doi.org/10.1016/S0079-1946\(98\)00040-8](https://doi.org/10.1016/S0079-1946(98)00040-8)
- Popp, T., Kern, H. & Schulze, O. (2001) Evolution of dilatancy and permeability in rock salt during hydrostatic compaction and triaxial deformation. *Journal of Geophysical Research: Solid Earth*, 106, 4061–4078. Available from: <https://doi.org/10.1029/2000JB900381>
- Robinson, A.H., Callow, B., Böttner, C., Yilo, N., Provenzano, G., Falcon-Suarez, I.H. et al. (2021) Multiscale characterisation of chimneys/pipes: fluid escape structures within sedimentary basins. *International Journal of Greenhouse Gas Control*, 106, 103245. Available from: <https://doi.org/10.1016/j.ijggc.2020.103245>
- Rutqvist, J. (2015) Fractured rock stress-permeability relationships from in situ data and effects of temperature and chemical-mechanical couplings. *Geofluids*, 15, 48–66. Available from: <https://doi.org/10.1111/gfl.12089>
- Serridge, C.J. & Cooper, A.H. (2022) Natural and anthropogenic halite karst subsidence in north Cheshire, UK; comparison of Rostherne Mere, Melchett Mere, Tatton Mere and their surroundings. *Quarterly Journal of Engineering Geology and Hydrogeology*, 56, Available from: <https://doi.org/10.1144/qjegg.2022-081>
- Shapiro, S.A. (2003) Elastic piezosensitivity of porous and fractured rocks. *Geophysics*, 68, 482–486. Available from: <https://doi.org/10.1190/1.1567215>
- Shapiro, S.A., Khizhniak, G.P., Plotnikov, V.V., Niemann, R., Ilyushin, P.Y. & Galkin, S.V. (2015) Permeability dependency on stiff and compliant porosities: a model and some experimental examples. *Journal of Geophysics and Engineering*, 12, 376–385. Available from: <https://doi.org/10.1088/1742-2132/12/3/376>
- Stoeckl, L., Banks, V., Shekhunova, S. & Yakovlev, Y. (2020) The hydrogeological situation after salt-mine collapses at Solotvyno, Ukraine. *Journal of Hydrology: Regional Studies*, 30, 100701. Available from: <https://doi.org/10.1016/j.ejrh.2020.100701>
- Stormont, J.C. (1997) Conduct and interpretation of gas permeability measurements in rock salt. *International Journal of Rock Mechanics and Mining Sciences*, 34, 303.e1–303.e11. Available from: [https://doi.org/10.1016/S1365-1609\(97\)00250-5](https://doi.org/10.1016/S1365-1609(97)00250-5)
- Stormont, J.C., Daemen, J.J.K. & Desai, C.S. (1992) Prediction of dilation and permeability changes in rock salt. *International Journal for Numerical and Analytical Methods in Geomechanics*, 16, 545–569. Available from: <https://doi.org/10.1002/nag.1610160802>
- Tarkowski, R. & Czapowski, G. (2018) Salt domes in Poland—potential sites for hydrogen storage in caverns. *International Journal of Hydrogen Energy*, 43, 21414–21427. Available from: <https://doi.org/10.1016/j.ijhydene.2018.09.212>
- Van Gent, H., Urai, J.L. & De Keijzer, M. (2011) The internal geometry of salt structures—a first look using 3D seismic data from the Zechstein of the Netherlands. *Journal of Structural Geology*, 33, 292–311. Available from: <https://doi.org/10.1016/j.jsg.2010.07.005>
- Wang, L., Liu, J., Xu, H. & Xu, Y. (2018) Research on confining pressure effect on mesoscopic damage of rock salt based on CT scanning. In: *Proceedings of GeoShanghai 2018 International Conference: Rock Mechanics and Rock Engineering*, Singapore. pp. 254–262. Available from: [https://doi.org/10.1007/978-981-13-0113-1\\_28](https://doi.org/10.1007/978-981-13-0113-1_28)
- Weisbrod, N., Alon-Mordish, C., Konen, E. & Yechieli, Y. (2012) Dynamic dissolution of halite rock during flow of diluted saline solutions. *Geophysical Research Letters*, 39, n/a–n/a. Available from: <https://doi.org/10.1029/2012gl051306>
- Yu, W., Huang, W., Liu, H., Wang, K., Wen, K., Gong, J. et al. (2020) A systematic method for assessing the operating reliability of the underground gas storage in multiple salt caverns. *Journal of Energy Storage*, 31, 101675. Available from: <https://doi.org/10.1016/j.est.2020.101675>
- Zhang, D., Skoczylas, F., Agostini, F. & Jeannin, L. (2020) Experimental investigation of gas transfer properties and stress coupling effects of



- salt rocks. *Rock Mechanics and Rock Engineering*, 53, 4015–4029. Available from: <https://doi.org/10.1007/s00603-020-02151-x>
- Zheng, Y., Zhao, Y., Ding, G., Wu, Z., Lu, S., Lai, X. et al. (2017) Solution mining technology of enlarging space for thick-sandwich salt cavern storage. *Petroleum Exploration and Development*, 44, 139–145. Available from: [https://doi.org/10.1016/S1876-3804\(17\)30018-6](https://doi.org/10.1016/S1876-3804(17)30018-6)
- Zidane, A., Zechner, E., Huggenberger, P. & Younes, A. (2014) Simulation of rock salt dissolution and its impact on land subsidence. *Hydrology and Earth System Sciences*, 18, 2177–2189. Available from: <https://doi.org/10.5194/hess-18-2177-2014>
- Zimmerman, R.W., Somerton, W.H. & King, M.S. (1986) Compressibility of porous rocks. *Journal of Geophysical Research: Solid Earth*, 91, 12765–12777. Available from: <https://doi.org/10.1029/JB091iB12p12765>
- Zivar, D., Kumar, S. & Foroozesh, J. (2020) Underground hydrogen storage: a comprehensive review. *International Journal of Hydrogen Energy*, 46, 23436–23462. Available from: <https://doi.org/10.1016/j.ijhydene.2020.08.138>

**How to cite this article:** Falcon-Suarez, I.H., Dale, M. & Marin-Moreno, H. (2024) Experimental study of geophysical and transport properties of salt rocks in the context of underground energy storage. *Geophysical Prospecting*, 1–17. <https://doi.org/10.1111/1365-2478.13516>